Noise-Free Estimation of Temporal Change in Seismic Wave Attenuation Using High-Stable Vibration Sources.

Shuhei Tsuji (shuhei.tsuji@gmail.com)
Nagoya Daigaku Daigakuin Kankyogaku Kenkyuka

Koshun Yamaoka
Nagoya University Graduate School of Environmental Studies: Nagoya Daigaku Daigakuin Kankyogaku Kenkyuka

Ryoya Ikuta
Faculty of Science, Shizuoka University

Full paper

Keywords: attenuation, amplitude, coseismic change, water injection, artificial seismic source, ACROSS

Posted Date: September 9th, 2020

DOI: https://doi.org/10.21203/rs.3.rs-70160/v1

Title page:

Title: Noise-free estimation of temporal change in seismic wave attenuation using high-stable vibration sources.

Author #1: (Corresponding Author) Shuhei Tsuji, Graduate School of Environmental Studies, Nagoya University, Furo-cho, Chikusa-ku, Nagoya 464-8601, Japan, stsuji@seis.nagoya-u.ac.jp

Author #2: Koshun Yamaoka, Earthquake and Volcano Research Center, Graduate School of Environmental Studies, Nagoya University, Furo-cho, Chikusa-ku, Nagoya 464-8601, Japan, kyamaoka@seis.nagoya-u.ac.jp

Author #3: Ryoya Ikuta, Faculty of Science, Shizuoka University, 836 Oya, Suruga, Shizuoka 422-8529, Japan, ikuta.ryoya@shizuoka.ac.jp

(go to new page)

Abstract

We developed a method to detect changes in attenuation in transfer functions obtained by precisely controlled artificial seismic sources, namely Accurately Controlled Routinely Operated Signal System (ACROSS), and applied it to monitor the temporal changes for in-situ data collected by previous studies. Our method, together with the usage of the ACROSS sources, is less susceptible to change in noise level to which conventional methods such as envelope calculation suffer. The method utilizes the noise level that is independently estimated in the frequency domain. Thus, we can eliminate the influence of the noise by subtracting it from the observed signal. To test the performance, we applied this method to a dataset obtained at Awaji Island, Japan from 2000 to 2001. We detected the changes in amplitude with several causes including ground motion in an earthquake and water injection experiment. At the 2000 Western Tottori earthquake (Mw = 6.6, Epicenter distance of 165 km), a sudden decrease in amplitude up to 5% followed by gradual recovery are clearly observed. These coseismic changes in amplitude are consistent with the opening of fluid-filled cracks as proposed by previous studies. We convert the amplitude change into ΔQ^{-1}, which gives similar

values as reported by previous studies using natural earthquakes. Increases in amplitude up to 5% associated with water injection experiments are also observed. During these experiments, the amplitude increased several days after the beginning of the injection and recovered to the previous level. This may be the result of a stress increase caused by the injection followed by a saturation increase by water diffusion.

Keywords

attenuation; amplitude; coseismic change; water injection; artificial seismic source; ACROSS

Main Text

Introduction

Temporal changes in the propagation property of seismic waves have been studied using both seismic velocity and attenuation. In previous studies coseismic changes, among others, draw the attention of researchers because they display clear synchronization to earthquakes and their relation to

46 relevant phenomena can be discussed quantitatively.

47 Coseismic changes in subsurface structure are often reported as
48 changes in seismic velocity. Various methods have been used to detect delays
49 in seismic velocity during earthquakes in many locations. Seismic
50 interferometry (e.g. Brenguier et al. 2008; Hobiger et al. 2016; Ikeda and Tsuji
51 2018), which does not need artificial sources, is generally used to measure the
52 temporal variation of seismic velocity in recent years. In contrast,
53 experiments with artificial seismic sources (e.g. Ikuta et al. 2002; Tsuji et al.
54 2018; Wang et al. 2020) are also carried out to identify coseismic velocity
55 changes with better resolution. In most cases the seismic velocity delays
56 during the earthquakes and recovers gradually over time. These phenomena
57 are accounted for with a fracturing of subsurface rock (Sawazaki et al. 2009;
58 Nakata and Snieder 2011) and/or crack opening by stress (Grêt et al. 2006;
59 Silver et al. 2007) or pore pressure changes (Ikuta and Yamaoka 2004;
60 Sawazaki and Snieder 2013) caused by the strong ground motions of
61 earthquakes.

62 The coseismic changes are also detected by changes in attenuation.
63 Temporal changes in the spectral ratio of natural earthquakes are often used
64 to estimate the change of attenuation (Chun et al. 2004; Titzschkau et al.
65 2010; Kelly et al. 2013). As the source amplitudes are difficult to estimate
66 precisely, spectral ratio is used assuming that the Q is independent of
67 frequency. Coda-Q has often been used to estimate the temporal variation of
68 attenuation in the region surrounding earthquake faults (Chouet 1979;
69 Huang and Kisslinger 1992; Sugaya et al. 2009) or in volcanic regions (Fehler
70 et al. 1988; Tonatiuh Domínguez et al. 2003). As the coda-Q reflects both
71 scattering and intrinsic attenuation, they also pay attention to the spectral
72 ratio in discussing intrinsic attenuation. In contrast to these studies,
73 Yamamura et al. (2003) revealed the periodic variation of attenuation
74 associated with earth tides using a piezo-electric actuator as a seismic source,
75 which produces seismic signals of constant amplitude. Despite the use of high
76 resolution seismic sources, no remarkable earthquakes occurred in their
77 experiment period and they did not detect a coseismic change of attenuation.

78 We have recently been developing effective methods to measure the
79 temporal change of amplitude of seismic signals observed by high stability
80 artificial sources. Here we show the result of the application of one of our
81 methods to the data set which includes the effects of strong earthquake
82 motions. We used the Accurately Controlled Routinely Operated Signal
83 System (ACROSS) as a high stability artificial source which makes it possible
84 to obtain accurate and stable transfer functions with adequate estimation of
85 noise level. ACROSS was developed for precise monitoring of propagation
86 property by means of continuous seismic waves excited by a precisely
87 controlled rotating eccentric weight (Kumazawa and Takei 1994), which
88 enables us to obtain transfer functions between sources and receivers
89 continuously and with precision (Kumazawa et al. 2007). With these
90 characteristics, ACROSS is able to monitor very small changes in the medium
91 in various fields, such as Sakurajima volcano, Japan (Yamaoka et al. 2014;
92 Maeda et al. 2015) or the Nankai trough subduction zone (Tsuji et al. 2018).
93 The data set used in this study was obtained in the experiment at

94 the Awaji site, western Japan (Ikuta et al. 2002; Ikuta and Yamaoka 2004),
95 where a surface fault appeared at the 1995 Hyogo-ken Nanbu Earthquake
96 (Kobe earthquake, M_{jma} 7.3) (Nakata and Yomogida 1995). At this site, an
97 experiment with two ACROSS vibrators was carried out from January 2000
98 to April 2001. They monitored change in travel time for P and S waves and
99 found coseismic changes in two earthquakes which caused relatively large
100 ground motion at the site (Ikuta et al. 2002; Ikuta and Yamaoka 2004). These
101 two earthquakes, the 2000 Western Tottori earthquake (WT) and the 2001
102 Geiyo earthquake (GY), had magnitudes and epicenter distances of M_W 6.6,
103 165 km and M_W 6.4, 215 km, respectively. Ikuta and Yamaoka (2004) proposed
104 a possible mechanism for these observations from the anisotropic changes of
105 transfer function and the strain change observed at a bore-hole strain meter
106 in the site. They interpret that the changes in the travel time were caused by
107 self-opening of the preferred oriented, fluid-filled cracks due to pore pressure
108 increase. Their interpretation indicates that changes in seismic attenuation
109 can be caused by friction loss of fluid in the cracks by the earthquake motion.

This is the direct motivation for this study.

Experiments at Awaji site

ACROSS experiments

First, we review the experiment that were carried out at Awaji site. Two ACROSS vibrators and two deep borehole seismometers were deployed at this site to monitor the temporal changes in the propagation property of the seismic wave (Yamaoka et al. 2001; Ikuta et al. 2002). The ACROSS vibrators were operated continuously for 15 months in the period from January 4, 2000, through April 9, 2001. The two ACROSS vibrators generated elastic waves with frequency modulation in different frequency ranges covering between 10 to 23 Hz. As the modulation period is 5 s, the sources produce discrete signals with an interval of 0.2 Hz in the frequency domain. Unlike recent experiments with ACROSS sources, no rotation switching had been implemented at that time, i.e. the weight rotates only clockwise viewing from the top throughout the experiment period. Seismic waves excited by the ACROSS vibrators are observed at the bottoms of two boreholes in the

127 experiment site. The seismometers in the boreholes are three-component
128 velocity-type sensors with a natural frequency of 3 Hz and 2 Hz for vertical
129 and horizontal components in the 800 m deep borehole, and 4.5 Hz for the
130 1700 m deep borehole. Both sensors are located almost vertically downward
131 from the sources with small horizontal distances of 50 m and 120 m from the
132 vibrators, respectively (Figure 1).

133 **Water injection experiments**

134 In this site, water injection experiments were conducted repeatedly
135 from 1997 to monitor a healing process in the Nojima Fault zone after the
136 1995 Kobe earthquake (Ando 2001). Water was pumped into the 1700 m
137 borehole to inject the water into the bedrock. The effects of injection are
138 monitored by a pressure gauge in the 800 m borehole, a strain meter at the
139 bottom of the borehole, and seismic stations around the site. An optical fiber
140 thermometer is deployed in the 1700 m borehole to measure the temperature
141 distribution in the well. During the injection, no appreciable change is
142 observed below a depth of 580 m, and Yamano and Goto (2001) conclude that
143 the water leaked out from a joint near the 540 m mark. A contraction of

144 approximately 10^{-8}–10^{-7} was observed by the strain meter at the 800 m
145 borehole (Mukai and Fujimori 2007). A cluster of earthquakes migrated with
146 the speeds of 20–80 m/h, which are interpreted as induced earthquakes
147 (Tadokoro et al. 2000). Hydraulic conductivity estimated by strain records
148 reduced by 50% from 2000 to 2003 (Mukai and Fujimori 2007), which are
149 interpreted as a healing of the fractures after the Kobe earthquake.

150 One of the water injection experiments was carried out in the
151 experiment period of ACROSS monitoring at this site. Four injection
152 operations were conducted. The 1st operation was performed on January 4,
153 2000, but was aborted due to the leaking of the water at the well top. The
154 2nd, 3rd, and 4th operations were performed in January 22–26, January 31–
155 February 5, and March 3–11, respectively, and were completed successfully.
156 The water was injected at constant pressures of 2.9, 4.0, and 4.5 MPa
157 respectively during each of the three operations. A total of 457 kL of water
158 was injected during the four operations (Nishigami 2001). Transfer
159 functions during the water injections were obtained only for the 800 m

borehole. The transfer function for the 1700 m borehole was hidden by the noise of the injection into the borehole. The analysis of the transfer function shows that the S wave travel time started to change after the beginning of the 2nd and the 4th operations and recovered before the end of each injection period (Yamaoka and Ikuta 2001).

Method

We estimated a temporal change in attenuation using a series of transfer functions that are obtained in Ikuta et al. (2002). In this study, we performed an independent data screening to remove the observation period in which ACROSS vibrators are not in proper operation. The first step of the data screening was conducted based on operation logs of the ACROSS source. Rotation frequency and mass position are logged in 1-s intervals and can be used to evaluate the quality of the operation. Cross covariance of the transfer functions for each 1-h interval with the reference time is also used for data screening in the second step. We removed the data for which the cross

176 covariances are less than 0.75. The low cross covariance may imply flaws in
177 the seismic observation systems.
178 After screening, the continuous wave records were divided into 100-
179 s segments which are stacked together in hourly intervals. The stacking was
180 carried out with a weighted average adopting the inverse maximum
181 amplitude in each segment as the weight. The stacked waveforms were
182 deconvolved with the source function of the force of the ACROSS vibrators
183 in the frequency domain to obtain transfer functions. As we used 100 s long
184 data for stacking, its Fourier transform contains spectral components with
185 an interval of 0.01 Hz. As the period of frequency modulation was 5 s, the
186 source signal gives spectral components with an interval of 0.2 Hz. This
187 causes an ACROSS source signal to appear every 20 components in the
188 frequency series for each vibration source. We refer to the components of the
189 ACROSS signal as signal channels. With the exception of the signal channels,
190 the components consist of noise referred to as the noise channel. We assumed
191 that the signal channels also contain noise whose variance is equivalent to

192 the mean of the variance of the two noise channels next to it.

193 We selected P and S waves in the transfer function in the time
194 domain, which is calculated by inverse Fourier transformation of the signal
195 channel. P and S waves were selected for the 800 m and 1700 m boreholes
196 in the same way as Ikuta et al. (2002) and Ikuta and Yamaoka (2004) for
197 comparison. The waveform including either P or S waves were selected with
198 a 20% Hanning window of 0.3 s centered at the travel time of P or S waves
199 estimated from the typical velocity of the country rock. P waves were
200 selected from the vertical components and S waves were selected from the
201 horizontal components (Figure 2). The transfer functions in the time domain
202 shown in Figure 2 was obtained by inverse Fourier transformation of those
203 in the frequency domain. P, S, and several later phases were identified in the
204 transfer functions for the seismometers in both the 800 m and the 1700 m
205 boreholes.

206 We estimated a temporal change in amplitudes of P and S waves
207 by calculating the ratio of the total energy of the ACROSS signal in

208 selected time windows of the 1-h transfer functions to those of the
209 reference transfer function. We selected the transfer function from 14:00 to
210 15:00 of January 19, 2000 as the reference transfer function as used in
211 Ikuta et al. (2002). The ratio r can be calculated as the following equation

212 $$r_l^2 = \frac{\sum_k (G_{kl} G_{kl}^* - \sigma_{kl}^2)}{\sum_k G_{k0} G_{k0}^*} \quad (1)$$

213 where G_{kl} denotes the Fourier transform of the transfer function extracted
214 by the windows in the time domain. σ_{kl}^2 denotes noise variance in the time
215 window. G_{k0} is the Fourier transform of the reference transfer function under
216 the same time window for G_{kl}. The subscripts k and l denote the frequency
217 component and calendar time, respectively. The method can avoid the
218 apparent change of signal amplitude caused by the changes of noise
219 amplitude, which conventional methods such as envelope calculation suffer.
220 This method takes the advantage of ACROSS in that noise level can be
221 estimated accurately.

222 The transfer functions and noise variance used in the equation (1)
223 for the selected windows including P and S waves are estimated based on

224 the method in Ikuta et al. (2002). The transfer functions G_k extracted with
225 the Hanning window onto the time domain data is calculated as equation (4)
226 in Ikuta et al. (2002) as follows:

227 $$G_k = \sum_{j=0}^{N} \frac{X_j}{S_j} H_{k-j} \quad (2)$$

228 where X_j and S_j is the j-th spectral component of the stacked
229 waveform and the source function, respectively. H_{k-j} is the $(k-j)$-th
230 component of the Fourier transform of the Hanning window. N is the
231 number of data in the frequency domain. Similarly, we can calculate noise
232 variance corresponding to each component of the transfer functions. The
233 noise variance extracted by the window function can be calculated as follows:

234 $$\sigma_k^2 = \sum_{j=0}^{N} \frac{\varepsilon_j^2}{S_j^2} H_{k-j}^2 \quad (3)$$

235 where ε_j^2 is noise variance at j-th frequency component.

236 We applied this method to the same data that are obtained by
237 Ikuta et al. (2002) at the Awaji site. However, we analyzed the signal of each
238 component of the seismometers instead of synthetizing the radial and

239 transverse component. Thus, we name two horizontal components as H1
240 and H2 for both sensors in the 800 m and 1700 m boreholes. H1 and H2
241 components in the 800 m borehole are directed N126°E and N216°E and
242 those of the 1700 m borehole are directed N90°E and N180°E. The S phase
243 that appears in each component is denoted S-H1 and S-H2.
244

245 ## Results

246 Temporal variation in amplitudes and travel times estimated for P, S-
247 H1, and S-H2 observed by the sensors in the 800 m and 1700 m boreholes are
248 shown in Figure 3. The variations of the amplitudes are calculated using the
249 method explained above for each component. We plot hourly data to show the
250 daily variations as well as long-term or event related variations. The travel
251 time variation is also calculated after Ikuta et al. (2002) for comparison. In
252 this plot, we calculated them for each component and showed hourly variation
253 instead of the plots as in Ikuta et al. (2002), which showed radial and
254 transverse components with a moving average over 24 h.

255

256 **Change in travel time**

257 We confirmed that the variation in the travel time is similar to

258 Ikuta et al. (2002). Estimated travel time is shown in the top three panels in

259 Figure 3. General trends in variation for the 800 and 1700 m boreholes are

260 quite similar. Long term variation for P and S waves such as gradual delay

261 from January to March in 2000, gradual recovery from April to May, and

262 gradual advance from July to September are observed. Sudden delay at

263 extremely heavy rain on September 11 is visible in all the components. The

264 delay is preceded by a two-month-long advance of travel time, which

265 corresponds to the dry summer season at this site. Coseismic delay and

266 gradual recovery are observed at the teleseismic event on October 6. In

267 addition, changes which may be associated with the 2nd and 4th water

268 injection experiments are clearly observed for the 800 m borehole, although

269 there is no mention of this event in Ikuta et al. (2002).

270

Change in amplitude

Several characteristics in the amplitude variation are seen throughout the experimental period (See the bottom three panels in Figure 3). The amplitude of the P wave for both the 800 m and 1700 m boreholes gradually decreased from January to February, shortly following the onset of the ACROSS experiment. The overall pattern of the amplitude variation of P waves is similar for both the 800 m and the 1700 m boreholes, although variation is larger in the 1700 m than that in the 800 m borehole. This may indicate that the region causing the attenuation change spreads below the sensor of the 800 m borehole as well as above it. Relatively large amplitude increases are observed for S-H2 of the 1700 m sensor from February to April.

Extremely heavy rainfall on September 11 changes the amplitudes suddenly for the S-H1 for both the 800 m and the 1700 m boreholes after a gradual change from the mid-August. They changed in the opposite direction. The amplitude decreases for the 800 m borehole after a gradual increase but increases for the 1700 m borehole after a gradual decrease. On the other hand, few changes can be seen in P and S-H2. In contrast to the amplitude change,

288 the travel time is delayed for both P and S waves. This change is interpreted
289 as the delay of the source motion with reference to the weight rotation caused
290 by energy dissipation immediately local to the source. It is difficult to
291 interpret the cause of the amplitude variation in terms of the source-ground
292 interaction only. It may be caused by the interference of multi-path waves
293 that suffer radiation variation near the source.

294 Diurnal variations that correlated well with the changes in
295 temperature (Figure 4), were also observed. For the 800 m borehole, the
296 amplitude has positive correlation with temperature for all the phases. The
297 P and S-H1 often show larger variation than that of the S-H2. The maximum
298 variation in the P and S-H1 reach approximately 5% and that of the S-H2
299 approximately 3%. For the 1700 m borehole, daily variation of P and S-H1 are
300 opposite to that of S-H2. P and S-H1 have positive correlation with the
301 temperature whereas S-H2 has negative correlation. The daily variation of P
302 (approximately 10%) is larger than that of S-H1 and S-H2 (approximately 3%).

303 On October 31, a step-like decrease in the amplitude of all the

304 phases for the 1700 m boreholes is seen. We checked total energy of the
305 transfer function in the frequency domain and found a step-like decrease in
306 energy at 08:00 on October 31. The ratio of this decrease is almost the same
307 for all the components. The level of ground noise of all the components of the
308 sensor were analyzed because we suspected that this change was caused by
309 a problem in the observation system, such as a change in amplification gain.
310 However, no significant difference in noise level was found except for a small
311 step-like increase of noise level in the UD component. The spectrum of the
312 noise also did not change at that time. This means that data-logging
313 instruments did not cause the signal decrease. The change might be caused
314 by a change in the coupling of the sensors against the well casing.
315
316 **Coseismic Change**
317 We analyzed the seismic changes caused by the Western Tottori
318 earthquake (WT) in 2000 and the Geiyo earthquake (GY) in 2001, as their
319 effect on the travel time is intensively discussed in Ikuta and Yamaoka (2004).
320 Figure 4 shows the temporal changes in amplitude during the ten

days before and after the earthquakes. The amplitude decreases at the earthquakes, and the change in amplitude at the WT earthquake is larger than the GY earthquake, which follows the same tendency as travel times. For the WT earthquake, a sudden drop of approximately 3% and 5% are observed in S-H2 for the 800 m borehole and S-H1 for the 1700 m borehole. Gradual recoveries lasted approximately one week after the earthquakes are observed in P and S for both boreholes (Figure 4a). The amplitude recovered to almost the same level as before the earthquake. However, for the GY earthquake, only S-H2 of the 800 m borehole shows a clear step-like decrease of 1% (Figure 4b). Gradual recovery is not observed in any phases of any sensors.

Change at water injections

Water injection causes a change in the transfer function both in amplitude and travel time (Figure 5). Significant increases in amplitude are observed in P and S-H1 of the 800 m borehole in the 2nd and 4th period of water injection. The magnitude of the change is up to approximately 3% for

both phases of the 2nd period and approximately 5% for both phases of the 4th period. Travel times of S-H1 and S-H2 also show advances in the 2nd and 4th periods of the injection experiment although neither Ikuta et al. (2002) nor Ikuta and Yamaoka (2004) noted these findings in their studies. The timing of the advances in the travel times are almost the same as those of the increase in amplitude. The period to the recovery is almost the same for S-H2 of travel time and P and S-H1 of amplitude. No significant change in amplitude and travel time is observed in the 3rd period.

Discussions

Interpretation of the change in amplitude

Fluid migration in cracks or pores is usually considered as a cause of attenuation. The effects of fluid saturation in attenuation have been widely studied with laboratory experiments. For example, Winkler et al. (1979) measured attenuation for dry, partially saturated, and fully saturated Massilon sandstone under several confining pressures. They demonstrated that the attenuation generally increases with saturation increase, and

355 decreases with an increase of confining pressure. The effect of confining
356 pressure is noticeable in saturated rocks. Pressure increase causes closure of
357 cracks or pores and thus, reduces the attenuation.

358 The change in amplitude in the water injection experiment can be
359 explained by a combination of saturation and pressure increase. The
360 amplitude observed in the 2nd and the 4th periods of the injection experiments
361 increased for several days following the beginning of the injection and then
362 returned to original levels. This observation may reflect a pressure increase
363 from the water injection from the well reducing attenuation along the ray
364 path, but diffusion of the injected water increased the fluid saturation in the
365 ray path region, increasing attenuation. However, if this mechanism operated
366 identically also in the 3rd period the amplitude should be increased. This
367 suggests the existence of other compromising factors.

368 The coseismic change in amplitude can be explained by the
369 mechanism proposed by Ikuta and Yamaoka (2004), where they explained
370 the delay of travel time during earthquakes with the opening of fluid-filled

371 cracks due to an increase in pore pressure caused by strong vibrations.

372 When new fluid-filled cracks are generated in the rock, viscous loss by the

373 fluid causes energy dissipation and increases attenuation.

374

375 **Comparison in terms of change in attenuation**

376 We try to convert the changes in amplitude to that of Q^{-1} for

377 comparison with coseismic changes observed in other studies. We assume the

378 amplitude ratio γ can be written as,

379 $$\gamma(f) = \frac{\frac{1}{d}A_0 \exp\left(-\frac{2\pi f d}{2c}Q^{-1}\right)}{\frac{1}{d}A_0 \exp\left(-\frac{2\pi f d}{2c}Q^{*-1}\right)} = \exp\left(-\frac{\pi f d}{c}\Delta Q^{-1}\right) \quad (4)$$

380 where, d is the distance of sensors from the source, A_0 is the amplitude at

381 the source, ω is the angular frequency of an elastic wave, c is the velocity of

382 an elastic wave, Q^{*-1} and Q^{-1} is the inverse of quality factor before and

383 after the earthquake. We put $\Delta Q^{-1} = Q^{-1} - Q^{*-1}$.

384 We may assume that the amplitude ratio we obtained in this study

385 α is equivalent to the amplitude ratio at the mean frequency used in our

386 experiment $\bar{f}$. Then, the change in ΔQ^{-1} can be written as follows:

$$\Delta Q^{-1} = -\frac{c}{\pi \bar{f} d} \ln(\alpha) \quad (5)$$

Herein, we assumed no velocity change in the equation because the coseismic velocity change is sufficiently small (<0.5%). With this method, the amplitude changes associated with the WT and GY earthquakes were converted into ΔQ^{-1} and compared with the changes in Q^{-1} that had been obtained in various regions by other methods. Table 1 shows the amplitude ratio of the transfer function before and after the earthquake obtained by the amplitude changes at the WT and GY earthquakes.

Table 1: Coseismic steps of amplitudes

	Step at WT		Step at GY	
	0800m	1700m	0800m	1700m
P-UD	0.95	0.94	--	--
S-H1	--	0.95	--	--
S-H2	0.97	0.97	0.99	--

Ratio of the amplitude of the transfer functions before and after the earthquakes in each sensor and each phase obtained by the comparison of the estimated change in amplitude. This corresponds to α in equation (4). "-" indicates that no significant change was observed.

401

402 We calculated ΔQ^{-1} by equation (5) using the amplitude ratio

403 shown in Table 1 and $V_P = 4.0\ [km/s]$, $V_S = 2.5\ [km/s]$. In this calculation

404 we put $f = 16$ [Hz] which corresponds to the center of the source frequency

405 of the ACROSS operation. The results are shown in Table 2, in which ΔQ^{-1}

406 are estimated in range of 1.0×10^{-3} to 1.0×10^{-2}.

407

408 **Table 2: ΔQ^{-1} obtained with equation (3)**

	Step at WT		Step at GY	
	0800m	1700m	0800m	1700m
P-UD	0.01	0.003	--	--
S-H1	--	0.002	--	--
S-H2	0.002	0.001	0.001	--

409 ΔQ^{-1} estimated with equation (5) under the assumption of $V_S = 4.0\ [km/s]$,

410 $V_P = 2.5\ [km/s]$) and $f = 16Hz$.

411

412 These ΔQ^{-1} are of the same order of magnitude as reported in the

413 previous studies with spectral ratio methods. For example, Kelly et al. (2013)

414 reported that ΔQ^{-1} in the fault region of the 2004 Parkfield earthquake (M_W

6.0) was of the order of 1.0×10^{-3}. Wang and Ma (2015) found a decrease in Q_S associated with the 1999 Chi-Chi earthquake (M_W 7.6). The Q_S was changed from 238 to 157, which corresponds to 2.2×10^{-3} of ΔQ^{-1}.

Conclusions

We developed a method to detect amplitude changes using a stable artificial seismic source, ACROSS, and applied it to in-situ data. The amplitude change was obtained by calculating the energy ratio of the transfer function of each period to that of a reference time. The energy of the noise is estimated to avoid apparent change in amplitude caused by noise level drift. We applied this method to the data acquired at the Awaji site by Ikuta et al. (2002). Various changes including the effects of water injection and strong ground motion by earthquakes are detected. An amplitude increase of 10% is observed associated with the water injection experiment. The changes in the water injection experiments can be explained by the changes in the degree of saturation of cracks in rocks. A coseismic decrease

of amplitude was observed for the 2000 Western Tottori earthquake and the 2001 Geiyo earthquake with a maximum decrease of approximately 10%. The coseismic changes can be explained by the mechanism proposed by Ikuta and Yamaoka (2004).

Declarations

Availability of data and materials

Please contact Dr. Ikuta Ryoya for the transfer functions and operation logs which we used for this analysis.

Precipitation and temperature data at Gunka station are retrieved from the JMA website (http://www.data.jma.go.jp/gmd/risk/obsdl/index.php , In Japanese)

Competing interests

The authors declare that they have no competing interests.

Funding

This study was founded by Nagoya University.

Authors' contributions

TS developed the method, carried out the analysis, and drafted the manuscript. YK supervised TS and developed the method together. IR provided the data of the experiments at Awaji Site and supported in developing the method. All authors read and approved the final manuscript.

Acknowledgements

We used meteorological data observed by an AMeDAS station managed by JMA. We would like to thank Editage (www.editage.com) for English language editing.

References

Ando M (2001) Geological and geophysical studies of the Nojima Fault from drilling:

463 An outline of the Nojima Fault zone probe. Isl Arc 10:206–214 .
464 https://doi.org/10.1111/j.1440-1738.2001.00349.x
465 Brenguier F, Campillo M, Hadziioannou C, Shapiro NM, Nadeau RM, Larose E (2008)
466 Postseismic relaxation along the San Andreas Fault at Parkfield from continuous
467 seismological observations. Science 321:1478–1481 .
468 https://doi.org/10.1126/science.1160943
469 Chouet B (1979) Temporal variation in the attenuation of earthquake coda near Stone
470 Canyon, California. Geophys Res Lett 6:143–146 .
471 https://doi.org/10.1029/GL006i003p00143
472 Chun K-Y, Henderson GA, Liu J (2004) Temporal changes in P wave attenuation in
473 the Loma Prieta rupture zone . J Geophys Res Solid Earth 109:1–15 .
474 https://doi.org/10.1029/2003jb002498
475 Fehler M, Roberts P, Fairbanks T (1988) A temporal change in coda wave attenuation
476 observed during an eruption of Mount St. Helens. J Geophys Res Solid Earth
477 93:4367–4373 . https://doi.org/10.1029/JB093iB05p04367
478 Grêt A, Snieder R, Özbay U (2006) Monitoring in situ stress changes in a mining

environment with coda wave interferometry. Geophys J Int 167:504–508 . https://doi.org/10.1111/j.1365-246X.2006.03097.x

Hobiger M, Wegler U, Shiomi K, Nakahara H (2016) Coseismic and post-seismic velocity changes detected by passive image interferometry: Comparison of one great and five strong earthquakes in Japan. Geophys J Int 205:1053–1073 . https://doi.org/10.1093/gji/ggw066

Huang ZX, Kisslinger C (1992) Coda-Q before and after the 1986 Andreanof Islands earthquake. Pure Appl Geophys 138:1–16 . https://doi.org/10.1007/BF00876711

Ikeda T, Tsuji T (2018) Temporal change in seismic velocity associated with an offshore MW 5.9 Off-Mie earthquake in the Nankai subduction zone from ambient noise cross-correlation. Prog Earth Planet Sci 5:62 . https://doi.org/10.1186/s40645-018-0211-8

Ikuta R, Yamaoka K (2004) Temporal variation in the shear wave anisotropy detected using the Accurately Controlled Routinely Operated Signal System (ACROSS). J Geophys Res Solid Earth 109:B09305. https://doi.org/10.1029/2003JB002901

Ikuta R, Yamaoka K, Miyakawa K, Takahiro K, Mineo K (2002) Continuous

495 monitoring of propagation velocity of seismic wave using ACROSS. Geophys Res
496 Lett 29:1627. https://doi.org/10.1029/2001GL013974
497 Kelly CM, Rietbrock A, Faulkner DR, Nadeau RM (2013) Temporal changes in
498 attenuation associated with the 2004 M6.0 Parkfield earthquake. J Geophys Res
499 Solid Earth 118:630–645 . https://doi.org/10.1002/jgrb.50088
500 Kumazawa M, Kunitomo T, Nakajima T, Tsuruga K, Hasada Y, Nagao H, Matsumoto
501 H, Kasahara J, Fujii N, Shigeta N (2007) JAEA-Research-2007-033.pdf. Tokai
502 Mura, Naka-gun, Ibaraki-ken, Japan
503 Kumazawa M, Takei Y (1994) Active method of monitoring underground structures by
504 means of Accurately Controlled ROtary Seismic Source (ACROSS). 1. Purpose
505 and principle. Abstruct Seismol. Soc. Japan p158
506 Maeda Y, Yamaoka K, Miyamachi H, Watanabe T, Kunitomo T, Ikuta R, Yakiwara H,
507 Iguchi M (2015) A subsurface structure change associated with the eruptive
508 activity at Sakurajima Volcano, Japan, inferred from an accurately controlled
509 source. Geophys Res Lett 42:5179–5186 . https://doi.org/10.1002/2015GL064351
510 Mukai A, Fujimori K (2007) Secular change of permeability in the fracture zone near

511 the Nojima fault estimated using strain changes due to water injection experiments.
512 Tectonophysics 443:193–199 . https://doi.org/10.1016/j.tecto.2007.01.023
513 Nakata N, Snieder R (2011) Near-surface weakening in Japan after the 2011 Tohoku-
514 Oki earthquake. Geophys Res Lett 38:1–5 . https://doi.org/10.1029/2011GL048800
515 Nakata T, Yomogida K (1995) Surface fault characteristics of the 1995 Hyogoken-
516 Nambu earthquake. J Nat disaster Sci 16:1–9
517 Nishigami K (2001) Summary of the wather injection experiment, shallow structure of
518 the Nojima fault and its healing process. Chikyu Mon 23:232–235
519 Sawazaki K, Sato H, Nakahara H, Nishimura T (2009) Time-lapse changes of seismic
520 velocity in the shallow ground caused by strong ground motion shock of the 2000
521 Western-Tottori earthquake, Japan, as revealed from coda deconvolution analysis.
522 Bull Seismol Soc Am 99:352–366 . https://doi.org/10.1785/0120080058
523 Sawazaki K, Snieder R (2013) Time-lapse changes of P- and S-wave velocities and
524 shear wave splitting in the first year after the 2011 tohoku earthquake, Japan:
525 Shallow subsurface. Geophys J Int 193:238–251 .
526 https://doi.org/10.1093/gji/ggs080

527 Silver PG, Daley TM, Niu F, Majer EL (2007) Active source monitoring of cross-well
528 seismic travel time for stress-induced changes. Bull Seismol Soc Am 97:281–293 .
529 https://doi.org/10.1785/0120060120
530 Sugaya K, Hiramatsu Y, Furumoto M, Katao H (2009) Coseismic change and recovery
531 of scattering environment in the crust after the 1995 Hyogo-ken Nanbu earthquake,
532 Japan. Bull Seismol Soc Am 99:435–440 . https://doi.org/10.1785/0120080012
533 Tadokoro K, Ando M, Nishigami K (2000) Induced earthquakes accompanying the
534 water injection experiment at the Nojima fault zone, Japan: Seismicity and its
535 migration. J Geophys Res Solid Earth 105:6089–6104 .
536 https://doi.org/10.1029/1999JB900416
537 Titzschkau T, Savage M, Hurst T (2010) Changes in attenuation related to eruptions of
538 Mt. Ruapehu Volcano, New Zealand. J Volcanol Geotherm Res 190:168–178 .
539 https://doi.org/10.1016/j.jvolgeores.2009.07.012
540 Tonatiuh Domínguez R, Fabiola Flores C, Gabriel Reyes D (2003) Temporal change in
541 coda wave attenuation observed at Volcán de Colima, México before the 1998
542 eruption. J Volcanol Geotherm Res 125:215–223 . https://doi.org/10.1016/S0377-

543 0273(03)00096-9

544 Tsuji S, Yamaoka K, Ikuta R, Kunitomo T, Watanabe T, Yoshida Y, Katsumata A

545 (2018) Secular and coseismic changes in S-wave velocity detected using ACROSS

546 in the Tokai region. Earth, Planets Sp 70:146 . https://doi.org/10.1186/s40623-018-

547 0917-2

548 Wang B, Yang W, Wang W, Yang J, Li X, Ye B (2020) Diurnal and semidiurnal P‐

549 and S‐wave velocity changes measured using an airgun source. J Geophys Res

550 Solid Earth 125:e2019JB018218. https://doi.org/10.1029/2019JB018218

551 Wang Y-J, Ma K-F (2015) Investigation of the Temporal Change in Attenuation Within

552 the Ruptured Fault Zone of the 1999 Mw7.3 Chi-Chi, Taiwan Earthquake. Pure

553 Appl Geophys 172:1291–1304 . https://doi.org/10.1007/s00024-014-0854-3

554 Winkler K, Nur A, Gladwin M (1979) Friction and seismic attenuation in rocks. Nature

555 277:528–531 . https://doi.org/10.1038/277528a0

556 Yamamura K, Sano O, Utada H, Takei Y, Nakao S, Fukao Y (2003) Long-term

557 observation of in situ seismic velocity and attenuation. J Geophys Res Solid Earth

558 108:1–15 . https://doi.org/10.1029/2002JB002005

559 Yamano M, Goto S (2001) Long-term temperature monitoring in a borehole drilled into
560 the Nojima Fault, Southwest Japan. Isl Arc 10:326–335 .
561 https://doi.org/10.1111/j.1440-1738.2001.00331.x
562 Yamaoka K, Ikuta R (2001) Observation of variation in seismic velocity assiciated with
563 the water injection experiments using ACROSS. Chikyu Mon 23:285–289
564 Yamaoka K, Kunitomo T, Miyakawa K, Kobayashi K, Kumazawa M (2001) A trial for
565 monitoring temporal variation of seismic velocity using an ACROSS system. Isl
566 Arc 10:336–347. https://doi.org/10.1111/j.1440-1738.2001.00332.x
567 Yamaoka K, Miyamachi H, Watanabe T, Kunitomo T, Michishita T, Ikuta R, Iguchi M
568 (2014) Active monitoring at an active volcano: amplitude-distance dependence of
569 ACROSS at Sakurajima Volcano, Japan. Earth, Planets Sp 66:32 .
570 https://doi.org/10.1186/1880-5981-66-32
571
572
573 # Figure Captions
574 - Figure 1

Location of Awaji site, epicenter of earthquakes, ACROSS vibrator, and borehole seismometers. Figures are from Figure 1 in Ikuta et al., 2004. (a) Location of the ACROSS site and epicenter of four earthquakes with strong ground motion during the ACROSS experiment. The open star indicates the location of the ACROSS at Awaji site. (b) Location of the ACROSS and borehole seismometers. The solid triangles show the location of 0800 m and 1700 m-deep boreholes. The onset map shows the details of the location configuration. The circles show seismometers in the borehole. (c) Cross section of the 800 m and 1700 m-deep boreholes.

- Figure 2

Reference transfer function in time domain and selected P and S phase for 800 m and 1700 m sensors. Transfer functions on 14:00 January 19, 2000 are used for the reference. Area with red background shows selected P and S phase for calculating the change in amplitude and travel time. We selected P waves from UD components (P-UD) and S waves from two horizontal components (S-H1 and S-H2).

591 ● Figure 3

592 Change in travel time and amplitude in all period. The changes in travel
593 time (yellow back) that are calculated after Ikuta et al., (2002) and
594 changes in amplitude (green back) that is obtained by the proposed
595 method. The center row indicates rainfall observed at Gunka station, the
596 nearest meteorological station. Periods with blue shading show the
597 periods of the water injection experiments. Red vertical lines show the
598 timing of the earthquakes mentioned in Ikuta and Yamaoka (2004).

599 ● Figure 4

600 Change in amplitudes approximately 10 days before and after the
601 occurrence of the 2000 Western Tottori (WT) earthquake and 2001 Geiyo
602 (GY) earthquake. The magnitudes and epicenter distances for WT and GY
603 are MW = 6.6, 165 km and MW = 6.4, 215 km, respectively. Bottom row
604 shows temperature at Gunka station.

605 ● Figure 5

606 Change in amplitude around the water injection experiments. The bottom

607 row shows the temperature observed at Gunka station. Blue background
608 indicates the periods of the injection experiments. In the period of the
609 water injection experiment, the transfer function of the 1700 m sensor
610 could not be analyzed because of the noise of the injection.

Figures

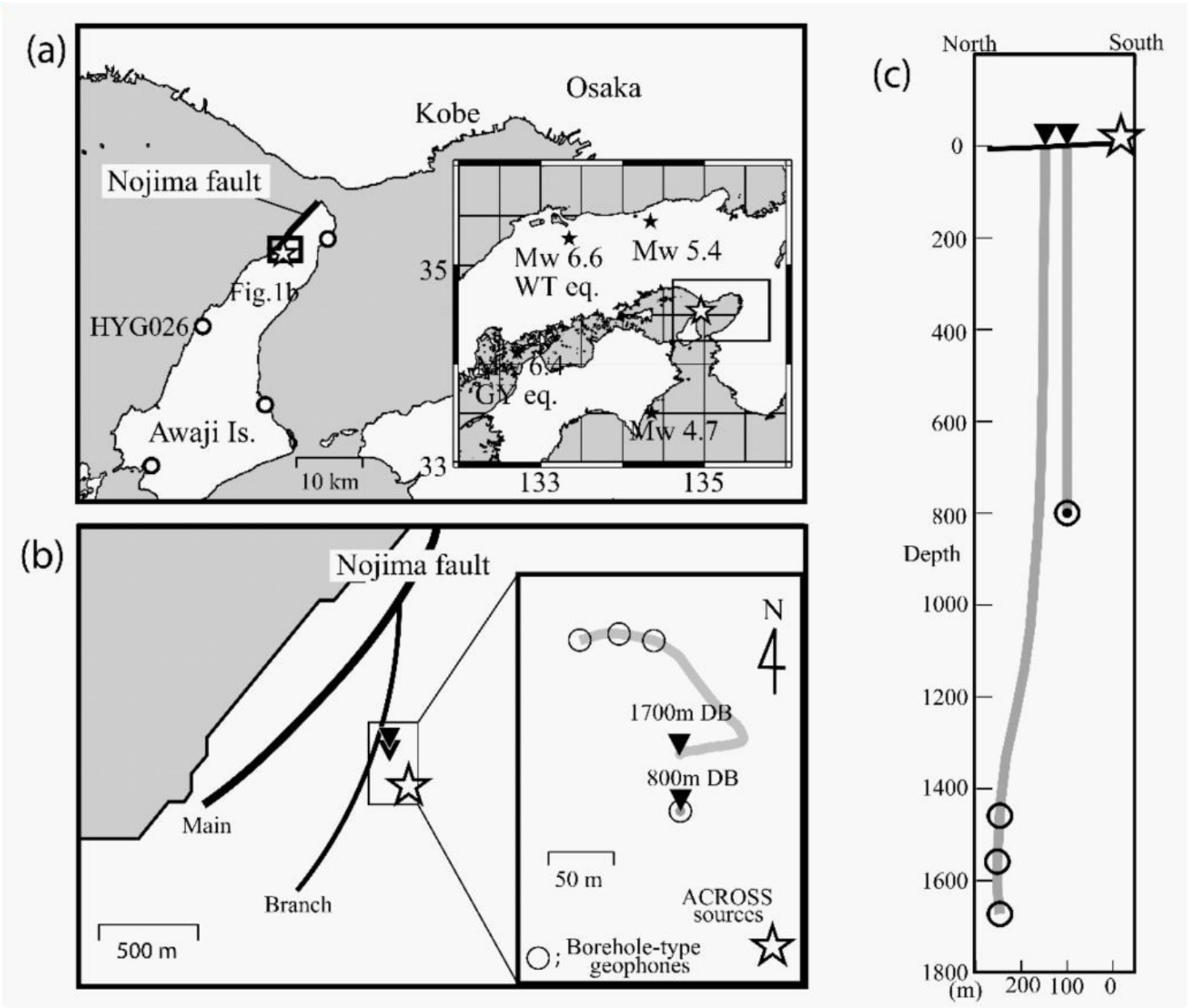

Figure 1

Location of Awaji site, epicenter of earthquakes, ACROSS vibrator, and borehole seismometers. Figures are from Figure 1 in Ikuta et al., 2004. (a) Location of the ACROSS site and epicenter of four earthquakes with strong ground motion during the ACROSS experiment. The open star indicates the location of the ACROSS at Awaji site. (b) Location of the ACROSS and borehole seismometers. The solid triangles show the location of 0800 m and 1700 m-deep boreholes. The onset map shows the details of the location configuration. The circles show seismometers in the borehole. (c) Cross section of the 800 m and 1700 m-deep boreholes.

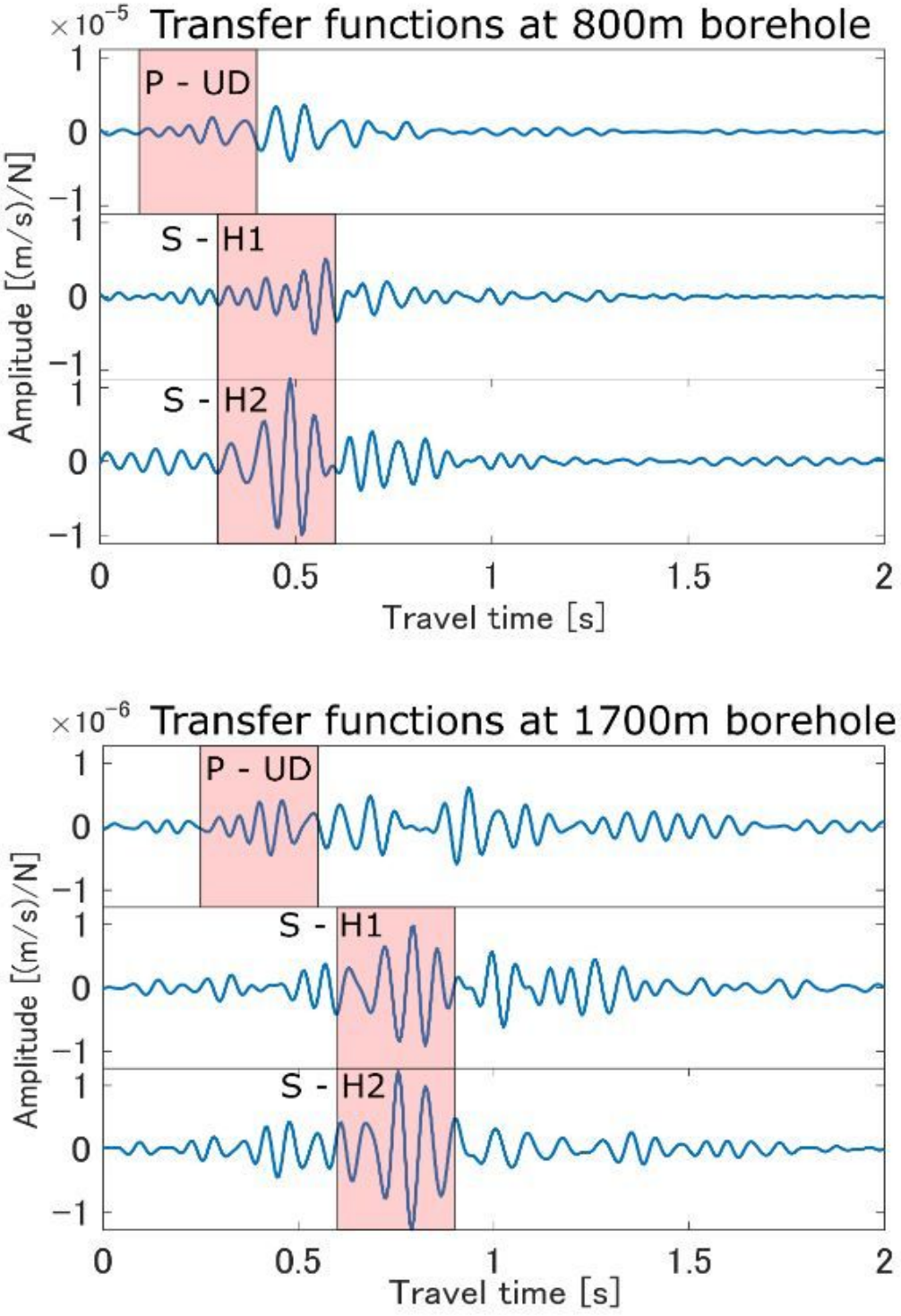

Figure 2

Reference transfer function in time domain and selected P and S phase for 800 m and 1700 m sensors. Transfer functions on 14:00 January 19, 2000 are used for the reference. Area with red background shows selected P and S phase for calculating the change in amplitude and travel time. We selected P waves from UD components (P-UD) and S waves from two horizontal components (S-H1 and S-H2).

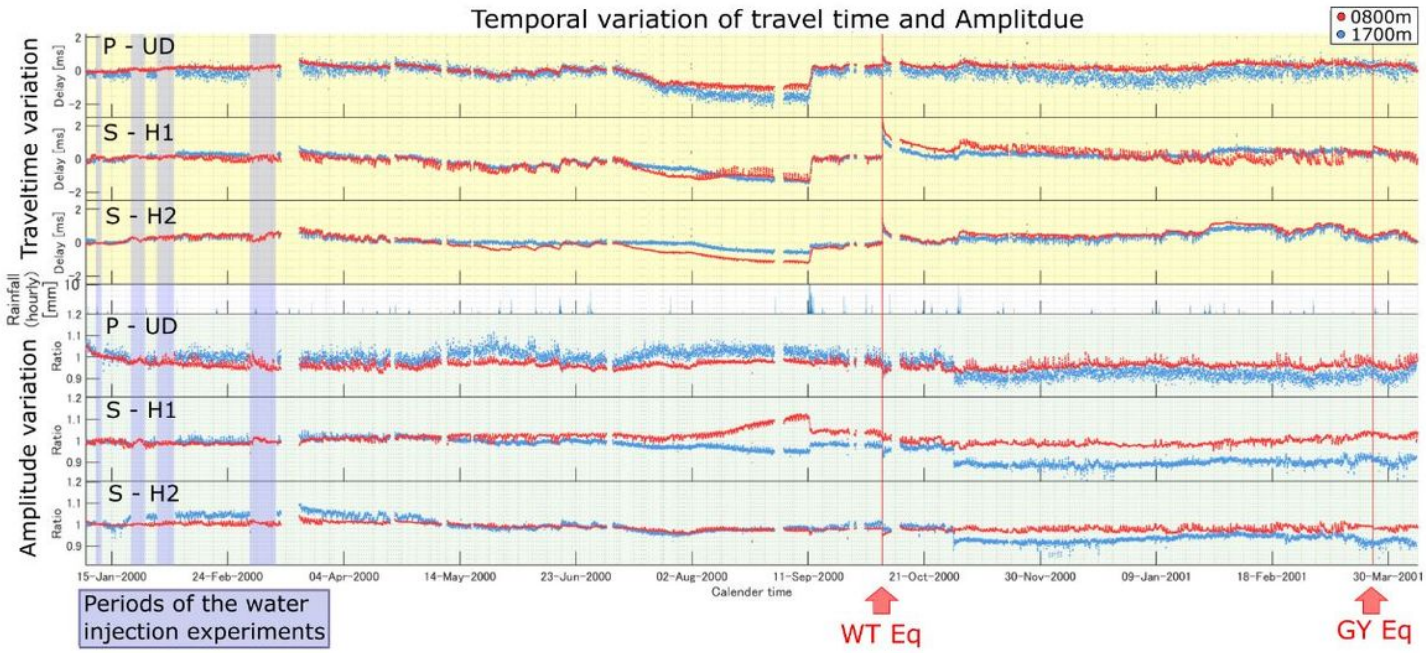

Figure 3

Change in travel time and amplitude in all period. The changes in travel time (yellow back) that are calculated after Ikuta et al., (2002) and changes in amplitude (green back) that is obtained by the proposed method. The center row indicates rainfall observed at Gunka station, the nearest meteorological station. Periods with blue shading show the periods of the water injection experiments. Red vertical lines show the timing of the earthquakes mentioned in Ikuta and Yamaoka (2004).

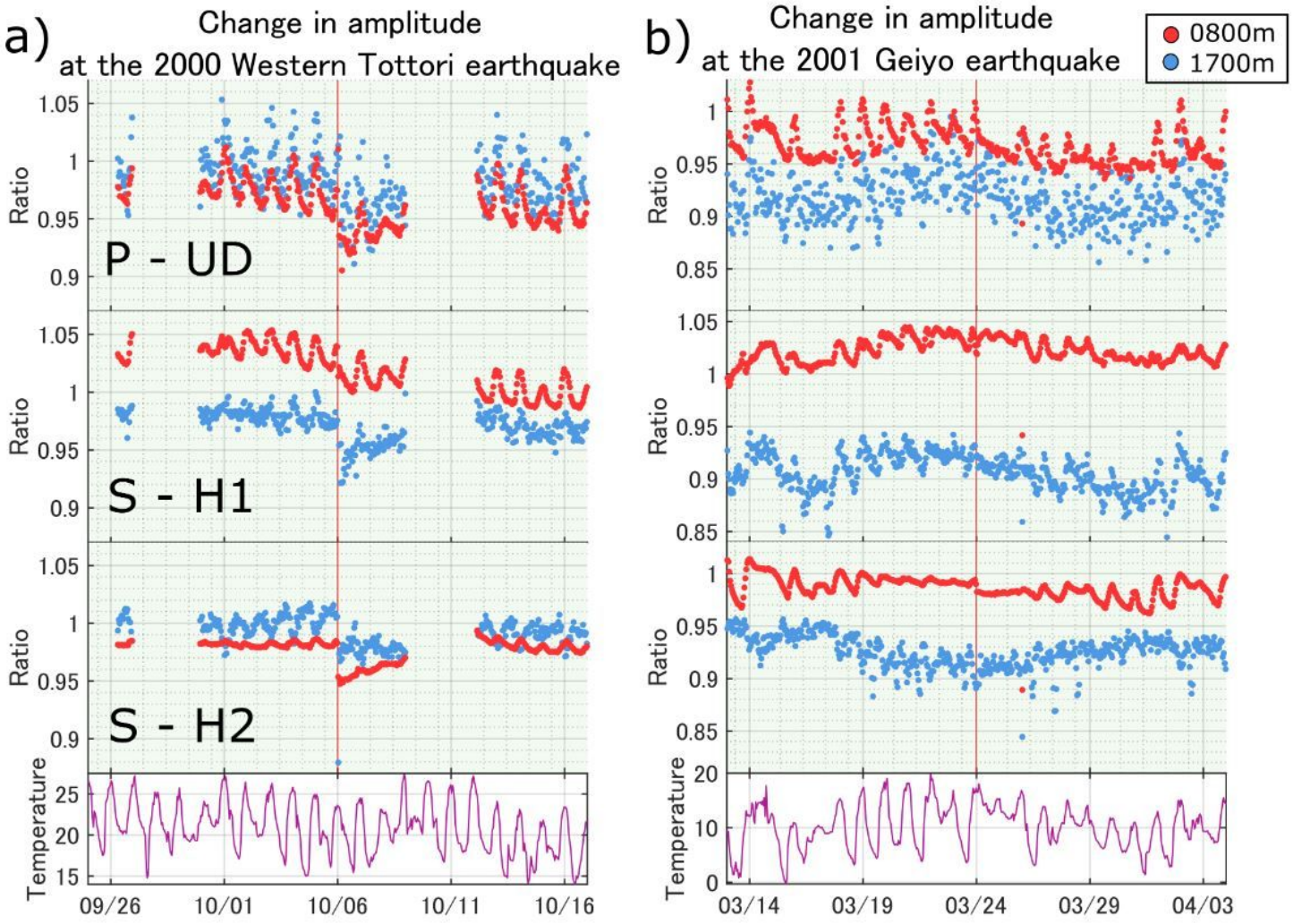

Figure 4

Change in amplitudes approximately 10 days before and after the occurrence of the 2000 Western Tottori (WT) earthquake and 2001 Geiyo (GY) earthquake. The magnitudes and epicenter distances for WT and GY are MW = 6.6, 165 km and MW = 6.4, 215 km, respectively. Bottom row shows temperature at Gunka station.

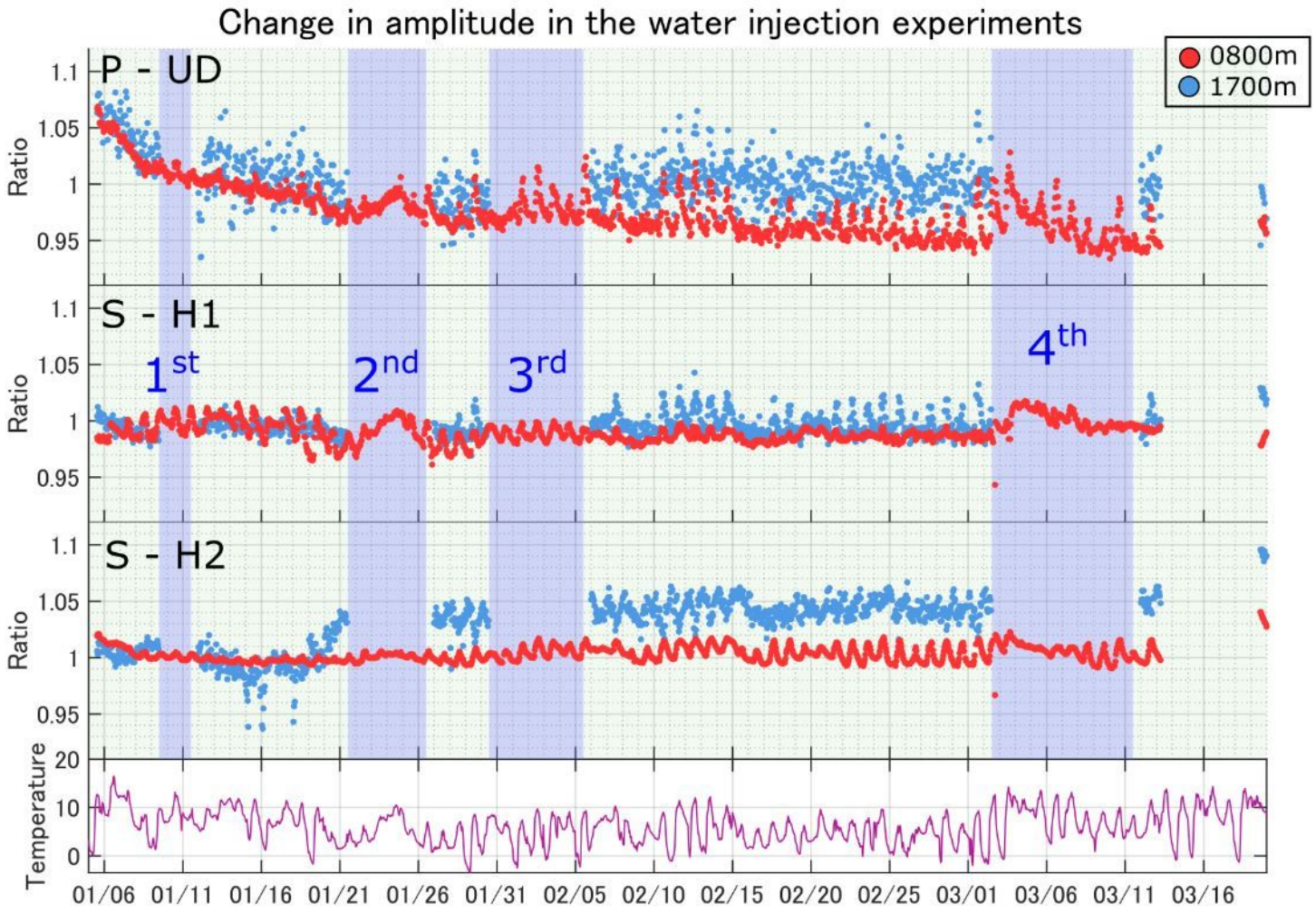

Figure 5

Change in amplitude around the water injection experiments. The bottom row shows the temperature observed at Gunka station. Blue background indicates the periods of the injection experiments. In the period of the water injection experiment, the transfer function of the 1700 m sensor could not be analyzed because of the noise of the injection.

Supplementary Files

This is a list of supplementary files associated with this preprint. Click to download.

- GraphicsAbstract.png